Research Article

The Synthesis of Lanthanum Oxide/Ni Catalyst on the CMK-3 for the CO$_2$ reforming of CH$_4$

Abbas Kakoo, Mardali Yousefpour *,

Faculty of Materials and Metallurgical Engineering, Semnan University, Semnan, Iran.

ABSTRACT

The catalysts with valve metals had been modified to use in the reforming process. Furthermore, there is a trend to the cheaper materials due to the deactivation and high price of the mentioned catalysts. In this case, at the present research work, the Nickel/CMK-3 catalysts with La$_2$O$_3$ as the promoter were synthesized by an impregnation method with 3 wt. % of La$_2$O$_3$. Also, the Nickel catalysts/CMK-3 and Nickel catalysts-La$_2$O$_3$/CMK-3 were characterized by N$_2$ adsorption-desorption, X-ray diffraction (XRD), Transmission electron microscopy (TEM), Field emission scanning electron microscopy (FE-SEM), Temperature programmed reduction (TPR), and the performance of the catalysts for CO$_2$ reforming of CH$_4$. In addition, the temperature programmed reduction (TPR) technique was selected to evaluate the catalyst properties for the CO$_2$ reforming of CH$_4$. In final, the obtained results demonstrated that the formation of amorphous mesoporous Carbon with NiO nanoparticles inside the channels of the supported base and also the Lantana oxide addition induced better Nickel oxide dispersion and increased the interaction of the catalyst particles with support. As a result, the Nickel catalysts supported on the Carbon mesoporous has shown enough activity for the CO$_2$ reforming of CH$_4$ at 650 °C. However, the mentioned samples were deactivated due to Carbon oxidation according to the TGA results. Therefore, the addition of La$_2$O$_3$ with 3 wt. % as a promoter improved the catalytic activity up to 57% and enhanced the catalytic stability at a duration time of 2 hr.

1. Introduction

In recent years, the Carbon dioxide reforming of methane has been paid more attention to Syngas production than the other reforming methods [1,2]. According to reaction (1), the CH$_4$ and CO$_2$ (Dry reforming reaction feed and greenhouse gases) convert to Syngas [3].

$$CO_2 + CH_4 \rightarrow 2H_2 + 2CO \tag{1}$$

The Syngas can be used to prepare a raw material for Fischer–Tropsch Synthesis to produce the Alkanes and Oxygenates materials [4,5]. The main disadvantage of Carbon dioxide reforming of CH$_4$ in industrial application is the deactivation of the catalysts due to the coke deposition on the surface catalysts. The catalyst modified with noble metal has been enough reviewed for reforming process [6]. In addition, metals ions loading, such as Ru, Ce, La, Y. etc. into the pores framework, is one of the excellent routes to provide the active sites [7-11]. So, having the fundamental knowledge of the metal ions effects as the promoter and their interactions with barriers is very noticeable. Yttrium and Yttria with high redox properties and chemical durability are also a proper candidate for the promotion of catalytic properties [12-15]. Costa et al. [16], examined the partial oxidation of methane by Pd/CeO$_2$ and Pd/Y$_2$O$_3$. They concluded that the selectivity to CO in Pd/Y$_2$O$_3$ catalyst

Corresponding Author: Mardali Yousefpour
Email: myousefpor@semnan.ac.ir

is higher than that of Pd/CeO_2. Because, Pd/Y_2O_3 catalyst facilitates the transformation of ethoxy species to the reforming reaction, however, Pd/CeO_2 catalyst leads to the high-speed oxidization of Carbon monoxide to Carbon dioxide. Wu et al. [17] reported an impregnated to synthesis the different Rh-supported catalysts in the reforming of methane. They found the order of catalytic activity as fallow: Rh/Y_2O_3 > Rh/CeO_2 > Rh/La_2O_3 > Rh/Al_2O_3. The activity of Rh/Y_2O_3 in the reforming route was modified due to the formation of the surface oxygen vacancies by Y_2O_3 [18]. Furthermore, Chen et al. studied the Cu effect on Ni-Cu bimetallic catalysts on YSZ base and reported the Cu addition induced the Ni-Cu alloy formation and the inhibition of coke formation in the reforming process [19]. Besides, Niazi et al. investigated the Cu, Mg, and Co effects on Ni/CeO_2 base in reforming reaction. They showed that the addition of the mentioned elements caused to improve the stability and selectivity of the catalyst [20]. However, the expensive cost and the deactivation of the catalysts with a noble element can be led a trend toward cheaper metals.

The deactivation of the catalyst is the Carbon deposition on the surface catalyst. As a result, it decreases the specific surface area, the active sites, and selective properties. Therefore, Nickel catalysts are preferred to other noble metal catalysts as they are cheaper, more active, and resistant to Carbon depositions in CO_2 reforming reaction [21]. Furthermore, the Carbon materials have been applied as catalysts or catalyst supports in the different processes due to having porosity or Oxygen surface groups, which can affect the selectivity and activity of the catalysts [22]. Therefore, a large number of Carbonaceous materials (Carbon black, activated Carbon, and the Carbon materials created from biomass remains) are investigated as the catalyst in the decomposition of methane gas [23]. Carbon-based catalysts are more beneficial than metal catalysts and Carbon-based catalysts due to having available, durable, and resistant to sulfur or other impurities [24-26]. In this case, Fidalgo et al. [27] studied the Carbon catalysts and microwave receptors in the CO_2 reforming of methane. They found that the oxidized Carbon observed on the surface of the catalysts happens under microwave heating, especially. Moreover, an important activity of CO_2 on the Carbon materials was reported. Jun et al. [28] applied La and Ce/CMK-3 as the catalysts for the CO_2 reforming of the CH_4 reaction. As a result, they reported that the ordered mesoporous Carbon materials, which were made of SBA-15 and KIT-6 hard Silica templates, could be used as the catalyst. The activity and stability of the catalyst doped with Ce and La on the CMK-3 base were higher as compared to the similar catalyst on the SBA-15 and KIT-6. Despite all of those, the research in the field of Carbon and Carbon catalysts in the CO_2

reforming of CH_4, the Nickel/CMK-3 catalysts have not been studied. Therefore, this research work was focused on the Nickel catalysts/CMK-3, and Nickel catalysts-La_2O_3/CMK-3 in the CO_2 reforming of CH_4, and the mentioned catalysts were synthesized and characterized.

2. Research Method and Materials

2.1. Preparation of precursors

The salt of $Ni(NO_3)_2 \cdot 6H_2O$ and $La(NO_3)_3.6H_2O$, Sucrose, and TEOS (Merck, 99%) were considered as the Nickel and Lanthanum, Carbon, and Silicon precursor. Furthermore, (Poly(ethylene glycol)-block-poly(propylene glycol)-block-poly(ethylene glycol), M=5800, Aldrich) and hydrochloride acid were used as the matrix and the pH stabilizer.

2.2. Synthesis of SBA-15

In the present work, Silica mesoporous is made as a hard template by using the hydrothermal route [29]. In the further step, the surfactant wax (8.0 g) is dissolved in the solution of deionized water (60 ml) and HCl (2M, 240 ml). Then, the TEOS (17 g) is added drop by drop to the mentioned solution at 40 ℃ and then is stirred vigorously for 24 hr. Subsequently, the obtained solution is transferred to a sealed Teflon vessel and dried at 100 ℃ for 24 hr. In the final step, the white powder is centrifuged, washed with deionized water, and heated at 90 ℃ until dehydrating. Then, the calcination treatment is carried out at 550 ℃ under the atmosphere conditions for 6 hr.

2.3. Synthesis of CMK-3

The replication method was used to form the combination of ordered mesoporous Carbon (CMK-3) and SBA-15. Furthermore, Sucrose was applied as a hard template and Carbon source according to method used by Gharahshiran et al. [25]. In this case, Silica (2.0 g) template was dispersed in the solution of Sucrose (2.5 g), H_2SO_4 (0.28 g, 98%), and deionized water (10 g). The mixture was heated at 100 ℃ for 6 hr in a heater and then the temperature was increased to 160 ℃ for 6 hr. The Silica template with partial polymerized and carbonized sucrose was heated again at 100 ℃ and then at 160 ℃ by a heater. In follow, the mixed solution of Sucrose (1.6 g), H_2SO_4 (0.18 g, 98%), and H_2O (10 g) was prepared. To complete the carbonization, the Sucrose-Silica composite was heated at 900 ℃ for 6 hr under the Argon atmosphere with a stream rate of 170 ml/min. Furthermore, hydrofluoric acid (5 wt. %) was used to remove the hard template of Silica at room temperature. In follow, mesoporous Carbon was filtered, washed with ethanol, and heated at 110 °C for 12 hr. To loading of Nickel (10 wt. %) into the mesoporous matrix, the impregnation method was used [30-31]. Subsequently, the heated Nickel catalyst was impregnated with $La(NO_3)_3.6H_2O$ (3 wt. %) in the

same way as the addition of La_2O_3, and two metal catalysts were heated at 90 °C similar to Ni catalysts as well. The schematic of synthesis of mesoporous Carbon and catalysts was shown in Figure 1.

2.4. Catalyst evaluation

The catalyst and promoter crystalline phase were studied using the X-ray diffraction analysis by a Bruker D8 diffractometer. The source of XRD analysis was carried out using the Cu-Kα radiation with λ=0.15418 nm and operated at 40 kV and 30 mA. Field emission electron scanning microscopy (MIRA3 TESCAN-XMU, FE-SEM) with an EDS detector was used for the observation of the morphology of the materials. A surface area analyzer (BEL, Sorp mini-II) was carried out to evaluate the N_2 adsorption/desorption isotherms of catalysts at 196 °C. The specific surface area calculation was determined using the Brunauer-Emmett-Teller (BET) technique. Furthermore, the pore diameter (DBJH) and pore volume were determined from the adsorption branch of isotherm curves by the conventional Barrett–Joyner–Halenda (BJH) method [32-33]. Before each test, the catalysts were heated to dry at 150 °C for 3 hr. The X-ray fluorescence examination was considered to evaluate the chemical compositions of the samples (ED, 2000 model, Oxford Co.). To take the TEM images, the samples were dispersed in an alcohol solution under ultrasonic conditions and thus a drop of the obtained solution was placed over the Carbon film grid to remove the water [34]. The reduction properties of the catalysts were studied using the temperature-programmed reduction analysis with a micrometric chemisorb2750. Subsequently, 50 mg of the sample was placed into the fixed-bath reactor and heated from 100 °C to 700 °C with a heat rate of 10 °C/min in the mixture of Hydrogen: Argon (10:90) atmosphere with a stream rate of 30ml/min. Before each test, the specimens were degassed in the Argon atmosphere at 250 °C for 1 hr. The thermogravimetric (L70/2171, Germany) analysis was applied to confirm the existence of Carbon element over the fresh catalyst. The H_2 depletion during the reduction process was evaluated using the gas chromatograph equipped with the thermal conductivity detector.

2.5. Activity study of catalysts

The catalytic activity was determined using a quartz tubular fixed bath continuous stream micro reactor (i.e. 8 nm) at different temperatures under atmospheric pressure. Then, the specimens with 10Nickel/CMK-3 and $3La_2O_3/10Ni/CMK-3$ were pressed, crushed, and separated from 40 to 60 mesh. Furthermore, a micro reactor was filled with the granules of catalyst in the constant weight (0.2g). In addition, before doing the catalytic reaction, the specimens were reduced in an atmosphere of pure H_2 with a stream rate of 30 ml/min at 700 °C for 3 hr. Then, the reactor was cooled to temperature of 500 °C [34]. In a final step, a mixture of reactants (CH_4 and CO_2 with: GHSV=12000ml/(h.g_{cat}), CO_2/CH_4=1:1, P=1atm) were transferred into micro reactor. The activity evaluation was carried out at different temperatures in the range of 500 to 700 °C with a rate of 50 °C/min. To remove the water from the specimens, they were sent to a water-trap chamber [34]. Subsequently, the chemical composition of the gas was evaluated using a gas chromatograph (HID YL-6100, with a carboxen 1010 column).
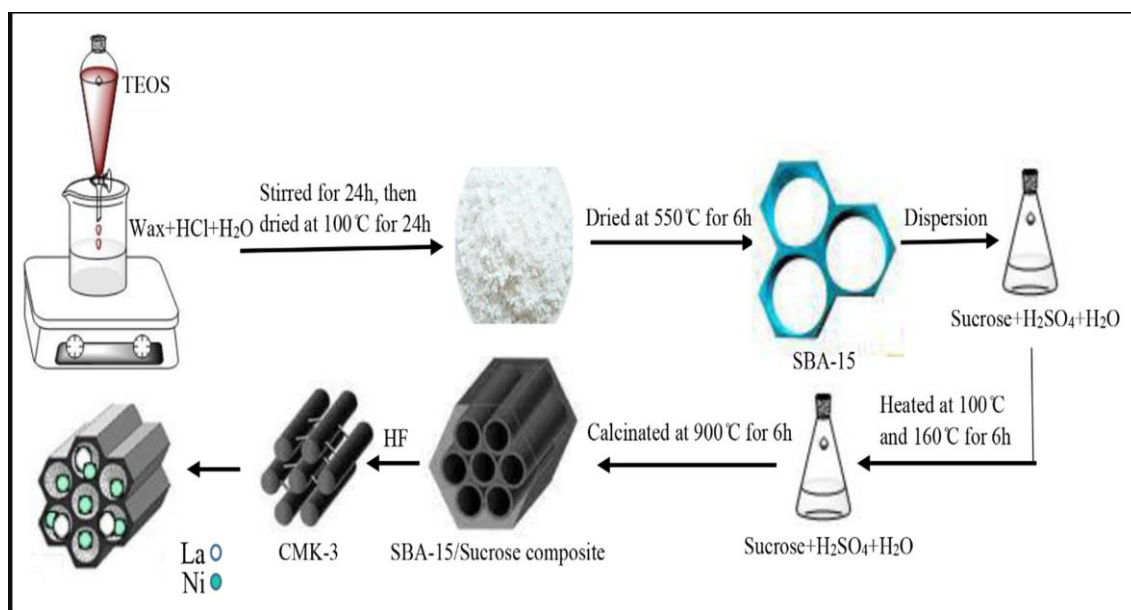

Figure 1. The schematic figure of the synthesis of mesoporous Carbons and catalysts.

3. Results and Discussions

3.1. Structural evaluation

The high-angle X-ray diffraction spectra from 10 to 70 degree for the Nickel catalysts/CMK-3 and Nickel catalysts-La$_2$O$_3$/CMK-3 is observed in Figure 2. As shown in Figure 2, the intensity of the peaks of specimens is in the range of 10 to 30 degree and is related to the amorphous mesoporous Carbon [33-35]. The XRD spectra of Ni-CMK-3 shows the three diffraction peaks at 2θ of 37.18, 43.31, and 62.77 degree; which are confirmed the NiO nanoparticles formation inside the support channels according to JCPDS 04-0835 standard. Furthermore, in the La$_2$O$_3$/Nickel-CMK-3 catalyst, similar to the Ni/CMK-3 catalyst, there are the main peaks of Nickel oxide. Additionally, any diffraction peak of La$_2$O$_3$ is not observed due to the low or well-dispersed non-crystalline phase of lanthanum oxide or the small crystallite size of oxides, which are out of the detection limit of the XRD analyzer [34].
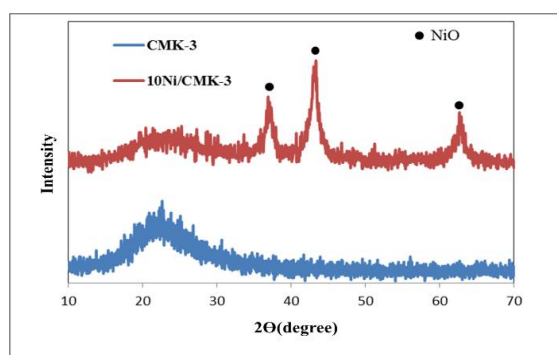

Figure 2. Intensity (a.u.) via 2Teta (degree) of CMK-3, 10Ni/CMK-3, 3La$_2$O$_3$/10Ni/CMK-3.

Besides, the textural details of fresh catalysts are observed in Table 1. The average size of Nickel oxides crystalline is determined using the following Scherrer equation:

$$D=(K\lambda)/(\beta cos\theta) \qquad (2)$$

In the Scherer relation, D is the average size of the crystalline grains, which is smaller or equal to the grain size; K is a dimensionless shape factor and can be assumed to be 1. λ is the wavelength of X-ray; β is the width of line broadening at the half of peak with maximum intensity and θ is the diffraction angle. The

XRD results indicated that the addition of La$_2$O$_3$ (3 wt%) decreased the Ni crystallite size and increased the dispersion of Ni particles (Table 1). The XRF examination data of the Ni/SBA-15/La$_2$O$_3$ catalysts are summarized in Table 1 (the weight percent of Ni less than 10% and the weight percent of La less than 3%). The results in Table 1 show some of the Nickel and La particles that are not wholly incorporated in the channels of the synthesized specimens. Also, the weight loss phenomena has happened in the duration of the washing treatment in the impregnation duration process. Furthermore, the oxide materials of Al$_2$O$_3$, P$_2$O$_5$, MgO, and Fe$_2$O$_3$ are in XRF data due to the existence of impurities in raw materials that are used to produce the samples.

Figure 3, shows the N$_2$ adsorption-desorption isotherms and pore size distribution spectra of the CMK-3 support, Nickel/CMK-3, and La$_2$O$_3$/Nickel-CMK-3 catalysts. The curves in Figure 3a and 3b display the classic type-IV of the N$_2$ adsorption-desorption isotherms with a perfect hysteresis loop, which indicate the formation and presence of the mesoporous materials.

In all samples, after loading the Ni and La$_2$O$_3$ inside the Silica template, the hysteresis loop is observed that has altered from H1 to H4 type. In the Nickel catalyst supported on Carbon mesoporous, the type of hysteresis loop is similar to the CMK-3 hysteresis loop, which is indicated by the CMK-3 mesoporous channels after loading of the Nickel (10 wt. %). However, in the La$_2$O$_3$/10Nickel-CMK-3 catalyst, the loop hysteresis is very weak. As a result, the adsorption branch over the desorption branch and the width of the loop hysteresis are very wide, which is expected a very border pore size distribution compared to the data reported in Table 2. Furthermore, Table 2 displays the results of the textural parameters of the S$_{BET}$, the volume of the total pore (V), average pore diameter (d), Nickel oxide crystallite size (d$_{NiO}$), and Nickel oxide dispersion (D$_{NiO}$). Thus, the results show the specific surface area, and the average pore volume of the CMK-3 support, which is reduced after the Nickel loading from 781 to 240 m^2/g and from 0.78 to 0.58 cm^3/g), respectively. However, the average pore diameter increases from 4 to 9 nm due to the filling of mesoporous of the CMK-3 matrix with Nickel oxide nanoparticles, which leads to the closure of the Carbon micro pores. Therefore, the larger average pore diameter is obtained due to the simultaneous reduction in the surface and pores volume, which is expected that most Nickel oxide nanoparticles are incorporated within the mesopores.

In comparison to the structural properties of the Nickel catalysts with and without a promoter, it can be concluded that the specific surface area of the modified catalyst with lantana has decreased.

Table 1. The composition of with and without promoter catalysts

NiO (%wt)	La$_2$O$_3$ (%wt)	Al$_2$O$_3$ (%wt)	P$_2$O$_5$ (%wt)	MgO (%wt)	Fe$_2$O$_3$ (%wt)	Sample
9.02	-	0.92	0.17	0.31	0.3	10Nickel/CMK-3
8.79	2.96	0.8	0.07	0.27	0.2	3La$_2$O$_3$/10Ni/CMK-3

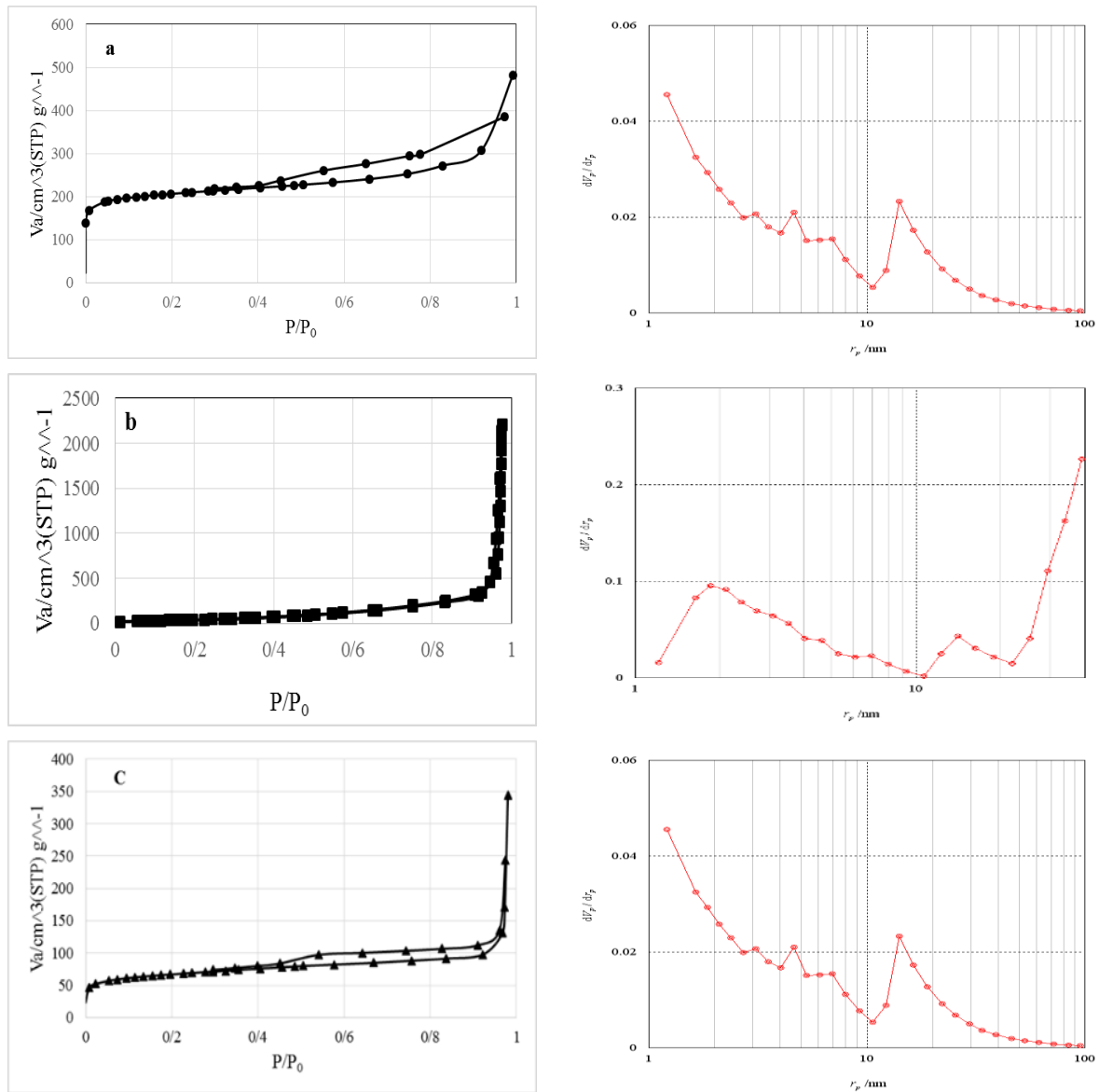**Figure 3.** a: Adsorption-Desorption Isotherms, BJH Adsorption pore size distribution in supported catalyst
b: CMK-3, 10Nickel/CMK-3, and c: 3La$_2$O$_3$/10Ni/CMK-3.

Table 2. The structural properties of the matrix with and without promoter catalyst

Surface area (m^2/g)	Average pore volume (cm^3/g)	Average pore diameter (nm)	NiO crystallite size (nm)	%Dispersion	Sample
781	0.73	3.8	-	-	CMK-3
239.7	0.53	8.86			10Nickel/CMK-3
175	49.3	9.77	6.7	5.13	3La$_2$O$_3$/10Ni/CMK-3

However, the amount of average diameter and the amount of volume of pores have increased. Furthermore, the size of the NiO nanoparticles at the catalyst decreases after the addition of Lanthanum oxide. In particular, the Lantana addition leads to better Nickel oxide dispersion and increases the interaction of the catalyst particles with the support.

Moreover, the loading of the Lanthanum oxide as a promoter can induce a further decrease in the amount of specific surface area, which is indicated by the addition of Lanthanum oxide and is induced the filling of more mesoporous channels. Therefore, the average pore volume is decreased. To know more details about Ni distribution over the 10Ni/CMK-3 and

3La₂O₃/10Ni/CMK-3 catalysts, TEM analysis is carried out to evaluate the primary sample of the catalysts. Then, TEM micro images of the catalyst specimens are presented in Figure 4.

In the CMK-3 support and unmodified Ni catalyst, a long uniform channel of the mesoporous can be observed at the highly ordered materials [29], which are known as the self-assemble of the mesostructured nanoparticles and a like-hierarchical structure [25]. These results are in agreement with the obtained results of the N₂ adsorption-desorption curves. Moreover, the semispherical Nickel oxide particles are well-dispersed on the surface of the mesoporous channels and inside the mesoporous channels [29].

Furthermore, Figure 4 shows the mesoporous Carbon materials, which are modified by La₂O₃. The main mechanism of the Lanthanum promoter is related to the roughness formation on the surface of the Nickel catalyst by providing the defects and disorders of network and then has an important role to control the activity and selectivity of the catalyst. As a result, the catalyst with La (3 % wt.) has the highest resistance to Carbon deposition due to the reduction in the size of the Nickel oxide particles, which prevents the creation and growth of the graphite. Therefore, it can be found that the main role of Lanthanum was the high nitrogen storage capacity of La₂O₃, which gasified the deposit of Carbon from methane decomposition reaction (Figures 4 and 5). Thus, less formation of Carbon and the best stability are obtained in the catalyst with the addition of La₂O₃ (3 % wt.). Furthermore, scanning electron microscopy images indicate the presence of the agglomerated nanometer particles in the matrix of metal particles (Figure 5).
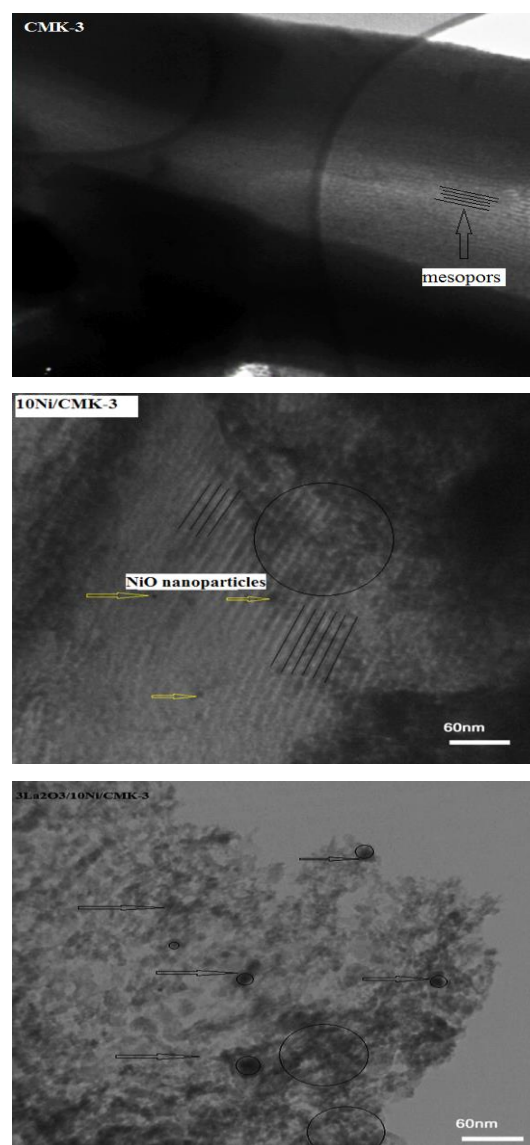

Figure 4. TEM micrographs of a: CMK-3, b: 10Nickel/CMK-3, and c: 3La₂O₃/10Ni/CMK-3.
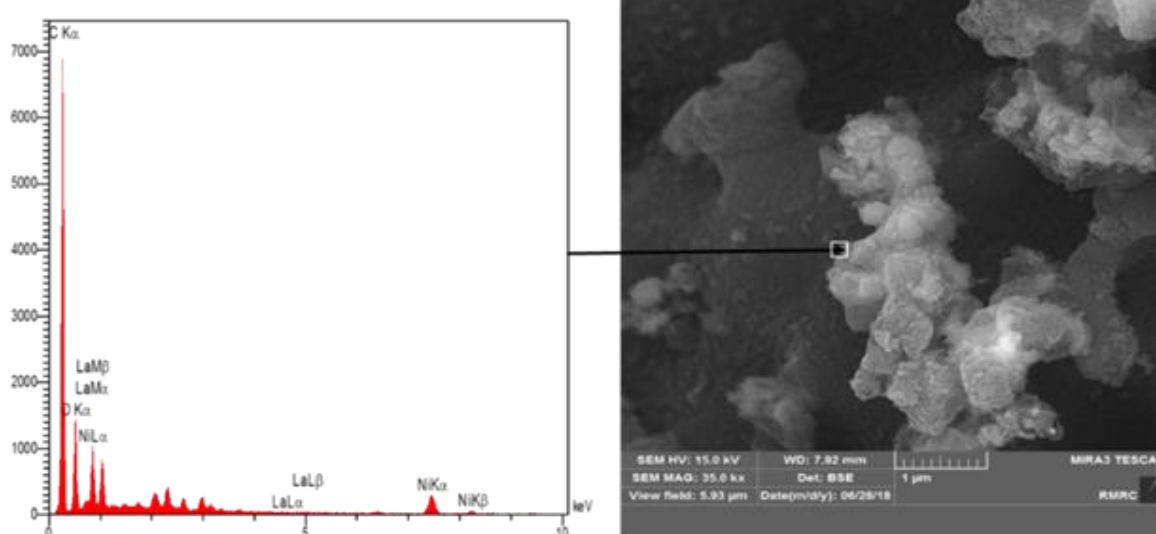

Figure 5. Image of Scanning electron microscope of 3La/10Nickel/CMK-3 sample

A semi-quantitative chemical analysis obtained with X-ray diffraction spectroscopy indicates the presence of elements (Table 3). A study on the reduction behavior of the catalysts and the TPR profiles for the Nickel catalysts with and without La_2O_3 (3 % wt.) is carried out and the results are presented in Figure 6. As shown in this figure, a reduction peak appears at the 400 °C in the Nickel/CMK-3. The Nickel oxide reduction point is appeared in the range of 300 to 400 °C as well [33]. Hence, the reduction point is observable at 400 °C, which is related to the NiO nanoparticles with relatively well-interacted in the support. In other words, the reduction of Nickel oxide into metallic Nickel has completely happened. In the TPR profile of $3La_2O_3/10Ni/SBA-15$, three peaks are appeared. In comparison to the Nickel catalyst, the first peak appeared at a lower temperature of 300 °C. Furthermore, the second peak at the average temperature from 400 °C to 500 °C and the third peak at 700 °C are observed.

Table 3. The percentage of weight elements specified with EDS analysis.

El.	C	O	Ni	La
W%	71.19	22.95	5.74	0.11

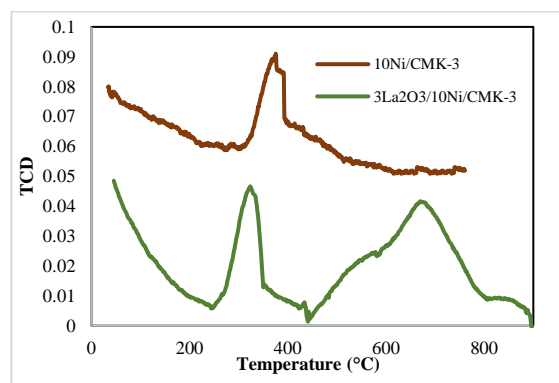**Figure 6.** H_2-TPR profiles of 10Nickel/CMK-3, $3La_2O_3/10Ni/CMK-3$.

As a final result, the first point had related to a reduction of the Nickel oxide with the weaker reaction with the support. Furthermore, the second point had attributed to the methane formation on the CMK-3 support according to the following reaction:

$$CO+3H_2 \rightarrow CH_4+H_2O \tag{3}$$

In addition, the third point had related to the stronger interaction between the lanthanum and the Nickel oxide. This means that the presence of the lanthanum oxide as a promoter facilitates the reduction of the Nickel oxide and thus the lanthanum oxide leads to the formation of the Ni-La solid solution phase with a stronger interaction with support, and then improves the thermal stability of the catalys [36].

3.2. CO_2 reforming of CH_4

To evaluate the dry reforming of CH_4, the catalysts are heated to 700 °C for 3hr, and then the temperature is decreased to 500 °C. Furthermore, the Hydrogen gas is injected during the evolution of Methane and Carbon dioxide conversion, and the temperature is increased in the range of 500 to 700 °C. Besides, the reactor tests are carried out in the same conditions for the Nickel catalysts/CMK-3 and Nickel catalysts-La_2O_3/CMK- 3. Thus, the results have demonstrated the activation of the Nickel catalysts with and without the Lanthanum oxide on CMK-3, which is started at 600 °C and below 600 °C. Therefore, Methane conversion and catalytic activity have not appeared in the mentioned conditions.

Moreover, the initial activity of both catalysts achieved at 600°C and reached near the maximum activity at 650 °C. Then, they were immediately deactivated after about one hour of reaction. In the previous research [25], the same results have been obtained for the La/CMK-3 and Ce-CMK-3 catalysts as well. The reason for the rapid deactivation of these catalysts can be attributed to various factors. The reactor tests shown that the thermal stability of the mesoporous Carbon support is weaker than the thermal stability of the mesoporous Silica supports at 700 °C. Thus, at the experimental evaluation, the problem of evaporation and burning of the Carbon support are observed at temperature up to 650 °C.

The results of the catalytic activity of the Nickel catalysts/CMK-3 and Nickel catalysts-La_2O_3/CMK-3 at 650 °C are reported in Table 4. Furthermore, the reverse water-gas shift reaction (RWGS) causes an increase to CO_2 conversion than CH_4 conversion for both catalysts. The molar ratio of H_2/CO in the CO_2/methane reforming of CH_4 must be equal to 1, which in this study is less than 1 for both catalysts. This molar ratio can be affected by the different reactions of RWGS for example; Boudwouard reaction and CH_4 decomposition. Therefore, in this work, the RWGS reaction can be induced the lower formation of the H_2/CO ratio. These results indicated that the addition of La_2O_3 as a promoter has a positive effect on promoting the catalyst performance than the unprompted Ni catalyst. The higher catalytic activity of La_2O_3 is incorporated into the Nickel/CMK-3 catalyst, and related to well-dispersed and excellent metal-support interaction [35].

Table 4. Methane and Carbon dioxide via temperature with: GHSV=12000ml/(h.g$_{cat}$), CO_2/CH_4=1:1, P=1atm.

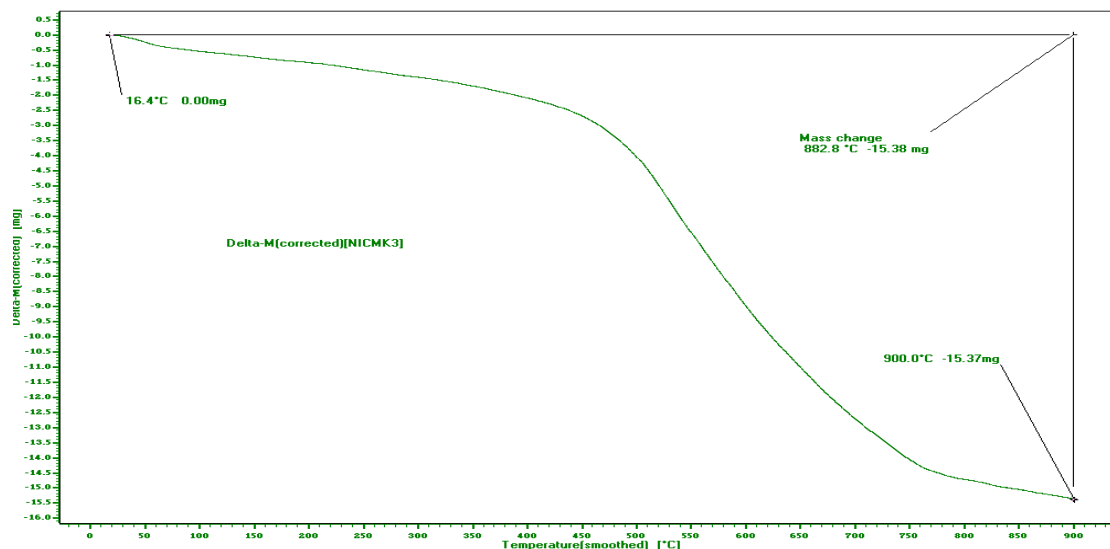| Samples	%CH$_4$ Conversion	%CO$_2$ Conversion
10Nickel/CMK-3	15.08	21.02
$3La_2O_3/10Ni/CMK-3$	35.1	40.14

Figure 7. TGA analysis of 10Nickel/CMK-3.

Figure 7 shows TGA graph of the Nickel catalyst. As shown in this figure, the weight loss via temperature is observed, which it has a low rate from room temperature up to 450 °C. However, weight loss is observed with a high slope above 450 °C. The evaluations show that a cation-free Nickel catalyst on the mesoporous Carbon without Lanthanum addition will be about 70% from room temperature to 900 °C. It is most likely due to the burning of Carbon in the vicinity of Oxygen under the TGA reaction conditions.

3.3. Catalytic stability

In the evaluation of the Ni catalysts supported on the Carbon mesoporous performance, it is observed that the Carbon mesoporous as support is not stable at temperatures above 650 °C and is evaporated and deactivated by rapid oxidation as shown in Figure 7.

Previously, there has not been published any result in the field of Methane dry reforming by the Nickel catalysts supported on the Carbon mesoporous. Similar results reported that the stability of the La and Ce catalysts supported on the Carbon mesoporous is about one hour at 650 °C [25]. In the present work, the stability examination is indicated by the Nickel/CMK-3 catalysts, which is not shown good stability. However, after adding Lanthanum oxide to the Nickel/CMK-3 catalyst, the catalyst stability is increased to two hours and then is suddenly deactivated.

Probably, the formation of an intermetallic phase of the Nickel-Lanthanum with a strong interaction with the support is formed with a higher thermal stability of the barrier. In addition, other factors such as the particles sintering of the catalyst, the Carbon deposition, and catalyst oxidation at the high temperature of the reaction can be caused a rapid deactivation of the catalysts supported on the Carbon mesoporous materials.

4. Conclusions

The Nickel catalysts/CMK-3 and the Nickel catalysts-La_2O_3/CMK-3 were synthesized by an impregnation route to use in the CO_2 reforming of CH_4. In comparison to the Nickel/CMK-3 and $3La_2O_3$/10Ni/CMK-3, according to the XRD spectra and Scherer equation, the most dispersion of the Nickel oxide and the minimum size of particle were related to the $3La_2O_3$/10Ni/CMK-3. Furthermore, the BET data was shown the addition of Lanthanum oxide, which reduced the surface area of the Nickel/CMK-3 catalyst. The TPR data revealed the addition of a promoter (3 % wt.) into the Nickel/CMK-3 catalyst, which changed the temperature reduction of the NiO to Ni^0 and enhanced the second temperature peak due to a well-interaction of the La_2O_3 with the support. According to the CO_2 reforming examination, the greatest catalytic activity and stability are related to the La_2O_3-promoted Nickel/CMK-3.

Acknowledgements

Conflicts of Interest

The author declares that there is no conflict of interest regarding the publication of this manuscript. In addition, the authors have entirely observed the ethical issues, including plagiarism, informed consent, misconduct, data fabrication and/or falsification, double publication and/or submission, and redundancy.

References

[1] Hu, Y.H. and Ruckenstein, E., 2004. Catalytic conversion of methane to synthesis gas by partial oxidation and CO_2 reforming. *Advances in catalysis*, *48*(1), pp.297-345.

[2] Pakhare, D. and Spivey, J., 2014. A review of dry (CO_2) reforming of methane over noble metal catalysts. *Chemical Society Reviews*, *43*(22), pp.7813-7837.

[3] York, A.P., Xiao, T.C., Green, M.L. and Claridge, J.B., 2007. Methane oxyforming for synthesis gas production. *Catalysis Reviews*, *49*(4), pp.511-560.

[4] Fan, M.S., Abdullah, A.Z. and Bhatia, S., 2009. Catalytic technology for carbon dioxide reforming of methane to synthesis gas. *ChemCatChem*, *1*(2), pp.192-208.

[5] Huang, J., Ma, R., Huang, T., Zhang, A. and Huang, W., 2011. Carbon dioxide reforming of methane over Ni/Mo/SBA-15-La_2O_3 catalyst: Its characterization and catalytic performance. *Journal of Natural Gas Chemistry*, *20*(5), pp.465-470.

[6] García-Diéguez, M., Finocchio, E., Larrubia, M.Á., Alemany, L.J. and Busca, G., 2010. Characterization of alumina-supported Pt, Ni and PtNi alloy catalysts for the dry reforming of methane. *Journal of Catalysis*, *274*(1), pp.11-20.

[7] Alvarez-Galvan, C., Melian, M., Ruiz-Matas, L., Eslava, J.L., Navarro, R.M., Ahmadi, M., Roldan Cuenya, B. and Fierro, J.L.G., 2019. Partial oxidation of methane to syngas over nickel-based catalysts: influence of support type, addition of rhodium, and preparation method. *Frontiers in Chemistry*, *7*, p.104.

[8] De Souza, T.L., da SILVA, V.S.T. and Cardozo Filho, L., 2015. Thermodynamic Analysis of synthesis gas production from autothermal reforming of mehane. *Blucher Chemical Engineering Proceedings*, *1*(2), pp.15460-15468.

[9] Nikolla, E., Holewinski, A., Schwank, J. and Linic, S., 2006. Controlling carbon surface chemistry by alloying: carbon tolerant reforming catalyst. *Journal of the American Chemical Society*, *128*(35), pp.11354-11355.

[10] Wang, Z., Xu, H., Zhang, Z., Wang, S., Ding, L., Zeng, Q., Yang, L., Pei, T., Liang, X., Gao, M. and Peng, L.M., 2010. Growth and performance of yttrium oxide as an ideal high-κ gate dielectric for carbon-based electronics. *Nano letters*, *10*(6), pp.2024-2030.

[11] Yan, Z., Xu, Z., Yu, J. and Jaroniec, M., 2015. Highly active mesoporous ferrihydrite supported Pt catalyst for formaldehyde removal at room temperature. *Environmental Science & Technology*, *49*(11), pp.6637-6644.

[12] Ballarini, A., Benito, P., Fornasari, G., Scelza, O. and Vaccari, A., 2013. Role of the composition and preparation method in the activity of hydrotalcite-derived Ru catalysts in the catalytic partial oxidation of methane. international journal of hydrogen energy, 38(35), pp.15128-15139.

[13] Kodo, M., Soga, K., Yoshida, H. and Yamamoto, T., 2010. Doping effect of divalent cations on sintering of polycrystalline yttria. Journal of the European Ceramic Society, 30(13), pp.2741-2747.

[14] Liu, H.M. and He, D.H., 2010. Physicochemical properties of Ni/Γ-Al_2O_3-Aln and effects of aln on catalytic performance of Ni/Γ-Al2O3-Aln in partial oxidation of methane. The Journal of Physical Chemistry C, 114(32), pp.13716-13721.

[15] Zhu, Q., Zhao, X. and Deng, Y., 2004. Advances in the partial oxidation of methane to synthesis gas. Journal of Natural Gas Chemistry. 13(4), p.191.

[16] Costa, L.O.O., Silva, A.M., Borges, L.E.P., Mattos, L.V. and Noronha, F.B., 2008. Partial oxidation of ethanol over Pd/CeO_2 and Pd/Y2O3 catalysts. Catalysis Today, 138(3-4), pp.147-151.

[17] Wu, X. and Kawi, S., 2010. Steam reforming of ethanol to H 2 over Rh/Y2 O3: crucial roles of Y2 O3 oxidizing ability, space velocity, and H_2/C. Energy & Environmental Science, 3(3), pp.334-342.

[18] Liu, H. and He, D., 2011. Properties of Ni/Y2O3 and its catalytic performance in methane conversion to syngas. *International journal of hydrogen energy*, *36*(22), pp.14447-14454.

[19] Chen, F., Tao, Y., Ling, H., Zhou, C., Liu, Z., Huang, J. and Yu, A., 2020. Ni-Cu bimetallic catalysts on Yttria-stabilized zirconia for hydrogen production from ethanol steam reforming. Fuel, 280, p.118612.

[20] Niazi, Z., Irankhah, A., Wang, Y. and Arandiyan, H., 2020. Cu, Mg and Co effect on nickel-ceria supported catalysts for ethanol steam reforming reaction. International Journal of Hydrogen Energy, 45(41), pp.21512-21522.

[21] Jabbour, K., El Hassan, N., Casale, S., Estephane, J. and El Zakhem, H., 2014. Promotional effect of Ru on the activity and stability of Co/SBA-15 catalysts in dry reforming of methane. International journal of hydrogen energy, 39(15), pp.7780-7787.

[22] Fidalgo, B. and Menendez, J.Á., 2011. Carbon materials as catalysts for decomposition and CO_2 reforming of methane: a review. Chinese journal of catalysis, 32(1-2), pp.207-216.

[23] Yousefpor, M., Tajally, M., Taherian, Z. and Khoshandam, B., 2021. A comparison of catalyst behavior of Samaria Modified Ni Catalyst Supported on Mesoporous Silica and Carbon for Methane CO_2 Reforming. Journal of Heat and Mass Transfer Research, 8(1), pp.105-113.

[24] Zhao, D., Feng, J., Huo, Q., Melosh, N., Fredrickson, G.H., Chmelka, B.F. and Stucky, G.D., 1998. Triblock copolymer syntheses of mesoporous

silica with periodic 50 to 300 angstrom pores. science, 279(5350), pp.548-552.

[25] Gharahshiran, V.S., Yousefpour, M. and Amini, V., 2020. A comparative study of zirconia and yttria promoted mesoporous carbon-nickel-cobalt catalysts in steam reforming of ethanol for hydrogen production. *Molecular Catalysis*, *484*, p.110767.

[26] Goscianska, J., Pietrzak, R. and Matos, J., 2018. Catalytic performance of ordered mesoporous carbons modified with lanthanides in dry methane reforming. *Catalysis Today*, *301*, pp.204-216.

[27] Fidalgo, B., Arenillas, A. and Menéndez, J.A., 2010. Influence of porosity and surface groups on the catalytic activity of carbon materials for the microwave-assisted CO_2 reforming of CH_4, Fuel, 89, 4002-7.

[28] Jun, S., Joo, S.H., Ryoo, R., Kruk, M., Jaroniec, M., Liu, Z., Ohsuna, T. and Terasaki, O., 2000. Synthesis of new, nanoporous carbon with hexagonally ordered mesostructure. *Journal of the American chemical society*, *122*(43), pp.10712-10713.

[29] Imperor-Clerc, M., Bazin, D., Appay, M.D., Beaunier, P. and Davidson, A., 2004. Crystallization of β-MnO_2 nanowires in the pores of SBA-15 silicas: in situ investigation using synchrotron radiation. *Chemistry of materials*, *16*(9), pp.1813-1821.

[30] Taherian, Z., Yousefpour, M., Tajally, M. and Khoshandam, B., 2017. Promotional effect of samarium on the activity and stability of Ni-SBA-15 catalysts in dry reforming of methane. *Microporous and Mesoporous Materials*, *251*, pp.9-18.

[31] Taherian, Z., Yousefpour, M., Tajally, M. and Khoshandam, B., 2017. A comparative study of ZrO_2, Y_2O_3 and Sm_2O_3 promoted Ni/SBA-15 catalysts for evaluation of CO_2/methane reforming performance. *International Journal of Hydrogen Energy*, *42*(26), pp.16408-16420.

[32] Rouquerol, J., Rouquerol, F., Llewellyn, P., Maurin, G. and Sing, K.S., 2013. *Adsorption by powders and porous solids: principles, methodology and applications*. Academic press.

[33] Cohen, E.R., Mills, I.M., Cvitas, T., Frey, J.G., Quack, M., Holström, B. and Kuchitsu, K. eds., 2007. *Quantities, units and symbols in physical chemistry*. Royal Society of Chemistry.

[34] Taherian, Z., Yousefpour, M., Tajally, M. and Khoshandam, B., 2017. Catalytic performance of Samaria-promoted Ni and Co/SBA-15 catalysts for dry reforming of methane. *International Journal of Hydrogen Energy*, *42*(39), pp.24811-24822.

[35] Li, J.F., Xia, C., Au, C.T. and Liu, B.S., 2014. Y_2O_3-promoted NiO/SBA-15 catalysts highly active for CO_2/CH_4 reforming. *International journal of hydrogen energy*, *39*(21), pp.10927-10940.

[36] Juan-Juan, J., Román-Martínez, M.C. and Illán-Gómez, M.J., 2009. Nickel catalyst activation in the carbon dioxide reforming of methane: effect of pretreatments. *Applied Catalysis A: General*, *355*(1-2), pp.27-32.

[37] Nabgan, W., Abdullah, T.A.T., Mat, R., Nabgan, B., Jalil, A.A., Firmansyah, L. and Triwahyono, S., 2017. Production of hydrogen via steam reforming of acetic acid over Ni and Co supported on La_2O_3 catalyst. *international journal of hydrogen energy*, *42*(14), pp.8975-8985.